Stellar Atmospheres of Nearby Young Solar Analogs

Eric J. Gaidos[12]
Division of Geological & Planetary Sciences
California Institute of Technology, Pasadena, CA 91125
gaidos@hawaii.edu
and

Guillermo Gonzalez[3]
Astronomy Department, University of Washington, Seattle, WA 98195-1580
gonzog@iastate.edu

ABSTRACT

High-resolution ($R \approx 90,000$) spectra of 34 nearby, young Sun-like stars were analyzed using stellar atmosphere models to estimate effective photosphere temperatures, surface gravities, and the abundance of certain heavy elements (C, Na, Mg, Si, S, Ca, Ti, Fe, and Ni). The effective temperatures derived from spectroscopy were compared with temperatures estimated using optical and near-infrared photometry. In many cases the spectroscopic temperatures are significantly higher than the photometric estimates, possibly as a result of spottedness or chromospheric activity on these active stars. Values of effective temperature, surface gravity, and luminosity were compared to theoretical stellar evolution tracks and the evolutionary status of these objects was evaluated. The correlation between heavy element abundance patterns and kinematics (space motion) was also examined. Two nearby stars that were tentatively assigned to the Hyades cluster based on kinematics have Fe abundances that are also consistent with membership in that cluster. Members of the Ursa Major kinematic group exhibit a range of [Fe/H] values but have monotonic [Si/Fe]. These two observations suggest that heterogeneous incorporation of the heavy elements into protostars is creating the variation in metallicity. Local Association members have a distinctly different Si/Fe that probably reflects their distinct origin and chemical inheritance.

Subject headings: stars: abundances, fundamental parameters, kinematics, planetary systems; PACS 97.10.Ex, 97.10.Jb, 97.10.Tk, 97.10.Zr

1. Introduction

Gaidos (1998) described a catalog of nearby young, solar-type stars selected as analogs of the Sun during early Earth history. These single or wide-binary stars are all within 25 pc and have spectral types G0-K2 and coronal X-ray luminosities suggesting ages less than 800 My (million years). Followup spectroscopy and photometery confirmed marked chromospheric activity, high lithium abundance, and rapid rotation, all indicative of stellar youth (Gaidos et al. 2000).

Detailed analysis of the spectra and spectral energy distribution of stellar photospheres can provide further constraints on the origin and evolutionary status of these objects. First, effective temperatures can be derived by comparing the equivalent widths of iron lines having differ-

[1]Visiting Astronomer, Kitt Peak National Observatory. KPNO is operated by AURA, Inc., under contract to the National Science Foundation.

[2]Current address: Department of Geology & Geophysics, University of Hawaii, Honolulu, HI 96822

[3]Current address: Department of Physics & Astronomy, Iowa State University, Ames, IA 50011

ent excitation energies with stellar atmosphere model predictions. Temperatures can be also estimated from photometry (i.e., colors) at optical and infrared wavelengths. Ideally, these two temperature estimates will be approximately the same (but see discussion below). The combination of effective temperature and luminosity (known by virtue of accurate *Hipparcos* parallaxes) allows the stars to be accurately placed in a Hertzsprung-Russell (HR) diagram where their locations can be compared with theoretical zero-age stellar isochrones. Accurate estimates of effective temperature are also required for the correct conversion of the equivalent width of the Li I line at 6708 Å into a lithium abundance and age proxy.

Second the abundance of heavy elements derived from the equivalent widths of absorption lines can be used, in principle, as a chemical "fingerprint" to relate stars to a common origin, either with other individual stars or with stellar clusters. This is potentially useful because the stars considered here are probably 100-800 My old and no longer physically associated with molecular clouds or stellar nurseries. Solar-mass stars (which do not produce significant amounts of heavy elements) forming from the same molecular cloud may have similar metal abundance patterns. For example, Perryman et al. (1998) report [Fe/H] values for 18 members of the nearby Hyades cluster with effective temperatures between 5000 and 6000 K. The mean metallicity is +0.13 with a RMS variation of 0.06, a dispersion consistent with the measurement accuracy. Varenne & Monier (1999) find a similar dispersion (but lower mean [Fe/H]) for Hyades F dwarf stars. In theory, stars from the same molecular cloud can also retain common space motions for $\sim 10^9$ yr until gravitational perturbations from the Galactic tide, molecular clouds, and other passing stars cause complete kinematic decoherence. Kinematic clustering is observed in this catalog (Gaidos 1998; Gaidos et al. 2000) and an objective of this work is to determine if there is a correlation between space common space motion and common metal abundance patterns.

2. Observations and Data Reduction

High-resolution ($R \sim 90,000$) spectroscopy was carried out at the Kitt Peak 0.9 m coude feed telescope with the echelle, F5 camera and 3K×1K Ford CCD during four observing runs (May, July, and November 1998, and March 1999). Typical total integration times were $\sim$ 1 hr per star. Spectral images were bias subtracted and flattened with quartz lamp flat fields, and charged particle events were removed by median filtering of multiple exposures. Individual spectral orders were extracted, corrected for sky emission, and wavelength-calibrated against thorium-argon arc spectra using the IRAF spectroscopic data reduction package. Equivalent widths were measured by hand using the IRAF spectrum analysis package. The atomic data for the 72 lines used in the analysis are given in Table 1.

Near-infrared magnitudes in the J, H, and K passbands (1.25, 1.65, and 2.2 μm) measured by the Two Micron All Sky Survey (2MASS) were extracted from the Infrared Science Archive (IRSA) using the Gator query engine. Additional near-infrared measurements were obtained from the Catalog of Infrared Observations, Version 4.1 (Gezari et al. 1993). Most stars also have 12 μm fluxes reported in source catalogs generated from observations by the Infrared Astronomical Satellite (*IRAS*) (Moshir et al. 1990). Visual (0.55 μm) magnitudes were obtained from the *Hipparcos* catalog (Perriman 1997).

3. Analysis

3.1. Spectroscopic analysis

The method of spectroscopic analysis employed in the present study follows that employed by Gonzalez et al. (2001) in their study of the solar-type parent stars of extrasolar planets. Briefly, we make use of equivalent widths (EW's) of relatively unblended Fe I and Fe II absorption lines with the Kurucz (1993) plane-parallel model atmospheres and the LTE abundance code MOOG, originally written by Sneden (1973), to determine the four basic atmospheric parameters (effective temperature, surface gravity, metal abundance, and microturbulence parameter) for each star. We adopted the atomic data in Gonzalez et al. and references cited therein. Although that model was calibrated for a different telescope-spectrograph combination, the agreement between the parameters of HD 10780 derived from these new data and those on which the model was originally calibrated

suggests no introduction of significant systematics (see §3.3). The uncertainty in each parameter was determined using the procedure described in Gonzalez & Vanture (1998). Values of the photosphere parameters and the number of Fe lines used are listed in Table 2. The abundances of other elements are also based on EW measurements and given in Table 4. The values for HD 1237, a far southern star, are taken from Gonzalez et al. (2001). An acceptable model fit to the data for HD 82443 could not be obtained: It appears that emission from the chromosphere of this very active star has significantly filled some photospheric absorption lines.

3.2. Photometric Temperature Analysis

Astronomical magnitudes were converted to fluxes using an empirical blackbody formulation of the infrared zero-magnitude fluxes that is accurate to 1%. Weighted least-aquare fits of theoretical Kurucz (1992) spectral energy distributions (SEDs) were made to the data: The two free parameters were the effective temperature $T_{\rm e}$ and the effective bolometric radius R of the star (the distance is fixed by the *Hipparcos* parallax). The Kurucz models are available for effective temperature increments of 250 K; interpolated models were constructed by a quartic temperature average of two adjancent models. (The derived temperature was found to be insensitive to the exact weighting scheme.) Most of the spectroscopically-estimated metallicities are within 0.1 dex of solar, therefore solar metallicity models were used. One-sigma (68.3% confidence) intervals for $T_{\rm e}$ and R were calculated using the method of constant χ^2 boundaries as described in Press et al. (1986), p. 532. Note that in some cases only two flux measurements (typically V and K) are available and $\Delta\chi^2$ but not χ^2 is properly defined. Only a very poor fit (reduced χ^2 of 10.8) could be achieved for the photometric data for HD 109011: Strassmeier et al. (2000) report that this object is actually a spectroscopic binary. The even poorer fit to the data on HD 220182 may demand a different explanation.

Although we neglect color corrections in our conversion of magnitudes (integrated over a pass band) to fluxes (at a single wavelength), these color corrections are relatively minor: We estimated the magnitude of these corrections by convolving the transmission data from representative filters (KPNO Harris V and 2MASS K_s) with the Kurucz SEDs of G0 and K2 stars, spectral types bracketing those of our program stars. In the case of the K_s band filter, a typical instrument response and atmospheric transmission was included. While our photometry is a heterogenous data set with different filters, detectors, and telescopes, these calculations are still appropriate to determine the representative magnitude of the color corrections. The difference in the color correction between the G0 and K2 stars is 0.006 magnitudes in the K_s bands and 0.067 magnitudes in the V-band. We estimated the worst-case effect of the latter on the photometric temperature estimate for a "typical" star (HD 20630). This was done by using *only* the V- and K-band data and varying the V magnitude by $\pm$0.033. This produced a variation in the estimated temperature of $\pm$50 K. Inclusion of additional data from other pass-bands into the model fitting will decrease such errors.

3.3. Comparison with previous results

Many stars in this study have been previously studied using photometry and spectroscopy and estimates of their photosphere parameters published. By and large, these previous estimates are in good agreement with our results. **HD 166:** Our spectroscopic estimate of $T_{\rm e}$ is significantly higher than a previous value (5255 K) derived from color indices and several temperature-sensitive lines (Zboril & Byrne 1998). **HD 1237:** The stellar parameters estimated by Santos et al. (2001) are consistent with the values reported here from Gonzalez et al. (2001). **HD 1835:** Cayrel de Strobel et al. (1997) (hereafter, C97) report six high-resolution spectroscopy measurements of atmospheric parameters with $T_{\rm e}$ ranging from 5673 to 5860 K, and Glushneva et al. (2000) derive 5669 K from JHK photometry. Our results (5675 K and 5792 K) are consistent with these values. **HD 10780** The spectroscopic and photometric $T_{\rm e}$ values and the metallicity are essentially identical to those derived from independent data and reported in Feltzing & Gonzalez (2001). The excellent repeatability may be related to the star's relatively low level of activity: In fact, Gaidos et al. (2000) concluded that despite its original selection based on X-ray emission, it is a solar-age star

and we have included it here only for completeness of the original sample. **HD 11131:** Our spectroscopic and photometric temperatures (5700 and 5629 K) are somewhat lower than those of C97 (5781 K) and Glushneva et al. (2000) (5645 K). **HD 20630 (κ Cet):** Ottmann et al. (1998) obtained atmospheric parameters at three rotational phases which average to $T_{\rm e}$ = 5680 K, somewhat lower than our value. **HD 30495:** Santos et al. (2001) find higher $T_{\rm e}$, log g, and [Fe/H] values but a similar microturbulence parameter. **HD 36435:** We did not observe this far southerly star but we include the spectroscopic results of Santos et al. (2001). **HD 43162:** Decin et al. (2000) estimate an effective temperature of 5593 K from photometry. Santos et al. (2001) found $T_{\rm e}$ = 5630, log g = 4.57, and [Fe/H] = -0.02, parameter values distinctly different from those obtained here. **HD 59967:** Blackwell & Lynas-Gray (1998) derive an effective temperature of 5732±52 K with the Infrared Flux Method (IRFM), while our photometric analysis gives a temperature of 5666 K with 68% confidence (1 σ) intervals of 5584-5752 K. Our spectroscopic temperature appears to be about 200 K warmer than ther IRTM estimates. **HD 72905 (π^1 UMa):** Our values for the four stellar parameters are identical, to within the uncertainties, with those of Ottmann et al. (1998). **HD 73350:** Our effective temperature and metallicity are identical to the values estimated by Favata et al. (1997). **HD 128987** Our effective temperature, metallicity, and microturbulence parameter are consistent with those derived by Feltzing & Gustafsson (1998). Our value for the surface gravity (log g = 4.49) is closer to their "photometric" (4.35) rather than their spectroscopic value (5.00). **HD 130948:** While our estimates of effective temperature and surface gravity agree with those of Chen et al. (2000), their metallicity ([Fe/H]=-0.20) and microturbulence parameters (2.0 km sec^{-1}) are significantly different. Hobbs (1985) estimates a roughly similar effective temperature of 5700 K based on photometery, but derives [Fe/H] = +0.20. **HD 152391:** Wyse & Gilmore (1995) estimate a metallicity [Me/H] of -0.08 based on *ubvy* colors, broadly consistent with our estimate of [Fe/H] = -0.02. **HD 206860:** Again, Chen et al. (2000) derive effective temperatures and surface gravities that are consistent with our results, but their [Fe/H] (-0.20) is much lower. The values of the microturbulence parameter (2.33 km sec^{-1}) that they derive for this star and for HD 130948 are implausibly high for a dwarf star and may be a consequence of sampling an inadequate range of line equivalent widths.

3.4. Comparison of Spectroscopic & Photometric Temperature Estimates

Twenty-five stars in our sample have effective temperature estimates based on both the spectroscopic and photometric methods. The spectroscopic estimates are, on average, 118 K higher than the photometric estimates. One possible explanation is that there are systematic errors in one or both of our two analyses. As shown in §3.2, the neglect of color corrections in our photometric temperature estimates cannot produce errors sufficiently large to explain the discrepancy. Furthermore, we see no trend of discrepancy with temperature. Of the 7 stars with temperature discrepancies exceeding 200 K, only two (HD 59967 and HD 128987) have published spectroscopic or photometric/IRFM temperature estimates (§3.3). Both of these estimates agree, to within the errors, with our own values. We also estimated a temperature from photometry of the active K dwarf ϵ Eri. Our estimate agrees with the spectroscopy-based effective temperature estimates of Drake & Smith (1993) and Santos et al. (2001), but is curiously higher than the values derived from narrow-band or broad-band photometry (Table 1 in Drake & Smith). Considering the general agreement of our results with other published results, we conclude there is no *a priori* basis for suspecting problems with our analyses.

A second explanation is that the spectroscopic temperature estimates are corrupted by non-thermal radiation related to stellar activity. The high surface magnetic fields on these active stars will power enhanced chromospheric emission and may affect magnetically sensitive lines such as that of Fe I at 6173 Å. Drake & Smith (1993) review evidence that chromospheric activity is responsible for, or at least associated with, an anomalously large line-to-line scatter in Fe abundance in solar-type photospheres. A large scatter could produce errors in stellar parameters derived from the relative equivalent widths of lines (e.g., temperature). Although such scatter is observed in spectra of the active K star ϵ Eri, neither Drake & Smith (1993)

nor Steenbock & Holweger (1981) could find a correlation between the abundance derived from a particular line and its Landé g factor. Drake & Smith instead suggest that some unknown non-thermal excitation or fluorescence effect may be involved. We find no correlation between the temperature discrepancy and indices of stellar activity (X-ray luminosity and Ca II HK line intensity). However, we discovered a significant correlation with surface gravity (Fig. 1). The trend of the temperature discrepancy with log g is consistent with the expected correlation between errors in spectroscopic temperature and errors in surface gravity, suggesting that deviations in the spectroscopic temperature from the true temperature of the star may play some role.

A third hypothesis is that the photometry is in error or that photometric estimates are affected by departures of the SED from the ideal Kurucz models. Some of the photometric temperature estimates rely on a V-band magnitude in addition to near-infrared photometry. *Hipparcos* visual magnitudes are unlikely to be in error by 0.1 magnitudes or more (Soderblom et al. 1998). Bell & Gustafsson (1989) concluded from theoretical model atmospheres that the $V-K$ colors of dwarf stars with temperatures ~ 5500 K are very weakly dependent (~ 0.02 mag) on surface gravity and metal abundance. They also found that the difference between the temperature estimates based on Johnson $V-K$ colors and the IRFM have an average of zero and a standard deviation of only 70 K.

A related hypothesis is that thermal emission from circumstellar dust increases the total flux from the star at near-infrared wavelengths and decreases the apparent photometric temperature of the star (the flux at optical wavelengths could be unaffected). Gaidos (1999) suggested that these stars, as potential young analogs to our Solar System, may harbor substantial dust clouds. Very roughly, the K-band flux of a 5500 K star would have to be augmented by 12% for its $V-K$ color to be consistent with a 5300 K star. The dust responsible for that emission, even at a maximum plausible temperature of 1500 K, would produce an 80% excess in the 12 μm flux relative to the photosphere. Such large excess emission has not been observed in data obtained by the Infrared Astronomical Satellite (IRAS) (Gaidos 1999) or by the Infrared Space Observatory (ISO) (Habing et al. 2001).

A fourth hypothesis is that the discrepancy between the two estimates is real and a consequence of the photometry measuring a disk-integrated temperature and spectroscopy measuring a value that is weighted towards the brightest parts of the disk. Large photospheric spots, typical on young stars, lower the V-band flux and hence the estimated photometric temperature. However, the required suppression of the V-band flux seems implausible: The most aggregious case is HD 52698 where the discrepancy between the temperature estimates is 280 K. Reconciling these two estimates requires that spots dim the V-band magnitude by 0.25 magnitudes (i.e., the $V-K$ color is reddened by 0.25 magnitudes). This can be produced by a single extremely large (r = 30 deg.) spot (Amando et al. 2000), but the absence of any modulation of the star's photometric light curve with this amplitude (Gaidos et al. 2000) requires that the effect would have to be produced by many, smaller spots. Furthermore, star spots contain more intense magnetic fields whose effect is to reduce the gas pressure and the effective surface gravity in the spots (Amando et al. 2000). More active, spotted stars should appear to have lower surface gravities, producing a negative correlation between surface gravity and the temperature difference. This is opposite to what is observed (Fig. 1). Finally, stellar spottedness is also correlated with stellar activity and a causal link between the temperature discrepancy and spots would be expected to produce correlations with stellar activity indices, an effect not seen.

4. Elemental Abundance Patterns

Iron: The distribution of our spectroscopically-determined [Fe/H] values for the young stars is plotted in Fig. 2. The distribution, with a mean of 0.02 dex and a standard deviation of 0.09 dex, peaks at solar metallicity and is essentially zero at ± 0.3 dex. In comparison, the [Fe/H] distribution of a volume-limited sample of 43 solar-mass field stars without detected planets (Santos et al. 2001) is bimodal and significantly broader (Fig. 2). The average [Fe/H] is -0.11 dex with a standard deviation of 0.18 dex. (Similarly, a subsample of 62 G dwarfs with

$T_e > 5250$ K from Favata et al. (1997) have a mean of -0.12 and a standard deviation of 0.25) The [Fe/H] distribution of the young star sample lacks a metal-poor tail and resembles the metal-rich moiety of the field star distribution. This is consistent with the combination of the first sample's narrower range of younger ages and the age-metallicity relationship in the galactic disk. Previous studies have also conclusively shown that stars with detectable planets are statistically more likely to have higher metallicities than similar "field" stars (Gonzalez et al. 2001; Santos et al. 2001). Of the three objects that are likely to be the most metal rich (HD 1237, HD 1835, HD 180161) one, HD 1237, is known to harbor a giant planet (Naef et al. 2001). Radial-velocity monitoring of HD 1835 places strict limits on the $m \sin i$ and semi-major axis of any substellar companions (Cumming et al. 1999). While the few available velocity measurements appear to rule out stellar companions around HD 180161 (Tokovinin 1992; Abt & Willmarth 1994; Gaidos 1998), high-precision doppler monitoring of this metal-rich star for planet detection is warranted.

Carbon: Carbon abundance is estimated from a single C I line and consequently has large uncertainties. The majority of the 29 stars with C I measurements appear to be carbon-poor relative to the Sun, with the exception of six stars with [C/Fe] > 0.2 (Fig. 3). These objects are certainly not classical carbon stars, evolved K and M giants with extremely red (> 2) $B - V$ colors and [C/O] ≥ 1 (Ohnaka et al. 2000). They generally do not have high abundances of the other elements. More likely, measurement of the equivalent width of the C I line was affected by nearby weak telluric (atmospheric water vapor) lines. The remaining 23 stars exhibit the well-known trend of decreasing [C/Fe] with increasing [Fe/H] (Gustafsson et al. 1999; King 2000). The best linear fit to the 23 points has a slope of -0.94 ± 0.25 and a χ^2 of 34.4.

Sodium: Values of [Na/Fe] have an average of -0.12 ± 0.01. The scatter of the values about the mean is consistent with the measurement errors ($\chi^2 = 21.6$, $N = 33$), and the data exhibit no significant trend over the observed range of [Fe/H]. Field stars with the same (solar) range of [Fe/H] have solar values of [Na/Fe] (Edvardsson et al. 1993; Tomkin et al. 1995). The apparent Na-poor character of the young solar analogs relative to older field stars is contrary to theoretical expectations: Galactic abundance evolution calculations suggest that averaged values of [Na/Fe] should increase with time and hence with [Fe/H] (Timmes et al. 1995). Such a trend with [Fe/H] has been confirmed by surveys of field stars (Edvardsson et al. 1993; Feltzing & Gustafsson 1998). A negative trend of [Na/Fe] vs. [Fe/H] described by Edvardsson et al. 1993 was not confirmed by Chen et al. (2000). However, Feltzing & Gustafsson (1998) describe a correlation with kinematics, such that solar metallicity stars with $Q_{\rm LSR} < 30$ km sec^{-1}, where $Q_{\rm LSR}$ is the total speed with respect to the Local Standard of Rest, have lower [Na/Fe] than their counterparts with higher space motions. Low-speed stars are statistically younger than their counterparts moving at higher speeds with respect to the LSR and this suggests that the positive correlation between [Fe/H] and [Na/H] is a kinematic, rather than chronological, relationship. All of these studies use the same Na I 6154/6160 Å line pair.

Magnesium: Most [Mg/Fe] values for the young solar analogs are subsolar, with an average value of -0.07 ± 0.02. There is no significant trend with [Fe/H] and no significant variation from the mean ($\chi^2 = 14.2$, $N = 32$). This is in contrast with various studies of field stars, which generally find [Mg/Fe] $\sim +0.1$ and significant scatter (Feltzing & Gustafsson 1998). Although, a subsolar [Mg/Fe] in this sample is consistent with the prediction that Fe production by Type I supernova will depress [Mg/Fe] in younger stars, models of Mg evolution in the galaxy generally fail to reproduce the observations (Timmes et al. 1995).

Silicon: [Si/Fe] values are derived from three high-quality lines (one is a doublet). The average [Si/Fe] for the sample is essentially solar (0.02 ± 0.01) and the negative trend with [Fe/H] is of low significance (-0.13 ± 0.12). (Note the small range of [Fe/H] spanned by the sample.) This negative trend is seen in both field stars (Edvardsson et al. 1993; Tomkin et al. 1995) and stars with detected planets (Gonzalez et al. 2001). This trend is most likely a consequence of Si being the product of massive stars and uncorrelated with Fe nucleosynthesis and thus the dilution of [Si/Fe] by higher [Fe/H]. The scatter about the mean is

comparable to the formal errors ($\chi^2 = 18.3$, N = 33).

Sulfur: Sulfur abundance is derived from the equivalent width of a single, weak line. The average of the available [S/Fe] measurements is solar (0.00 ± 0.03) and the scatter is consistent with the measurement errors ($\chi^2 = 35.9$, N = 19).

Calcium: [Ca/Fe] estimates are also derived from high quality lines. The average relative abundance is identical to that of Si (0.02 ± 0.01). There is also a negative trend of marginal significance(-0.16 ± 0.14) with [Fe/H] (Fig. 5).

Titanium: The value of [Ti/Fe] averaged over the sample is approximately solar (-0.02 ± 0.01) and the individual measurements exhibit no significant trend with [Fe/H]. The scatter about the mean is consistent with the measurement errors ($\chi^2 = 24.2$, N = 33).

Nickel: Nickel abundances among the young solar analogs are decidedly subsolar; (mean value of -0.15 ± 0.02) and exhibit a strong positive trend with [Fe/H] (slope of 0.60 ± 0.22) (Fig. 6). Edvardsson et al. (1993) report [Ni/Fe] values with an average of 0.00 ± 0.03 over the entire metallicity range and no significant correlation with [Fe/H]. The isotopes ^{56}Ni and ^{58}Ni dominate the composition of elemental nickel and are produced in massive stars and in Type Ia (deflagration) supernovae. Galactic abundance evolution calculations (Timmes et al. 1995) in which most of the Ni is produced in massive stars, are in accord with the observations of Edvardsson et al. (1993). However, the theory also predicts an overabundance of Ni (relative to solar) by a factor of 3-4 for the time when and location where the Sun formed. The positive trend with [Fe/H] observed here and by Gonzalez et al. suggests that for some stars the contribution by Type Ia supernovae may be significant.

5. Discussion

5.1. HR Diagram

The original selection criteria for young solar analog candidates included the requirement that they lie on or near the Zero Age Main Sequence (ZAMS) for solar-like metallicities in a Hertzsprung-Russell (HR) diagram (Gaidos 1998). At that time, precision estimates of photosphere parameters were not available for most candidates and $B - V$ color was used as a proxy for effective temperature. Here, we compare photometrically and spectroscopically derived parameters (luminosity and effective temperature) with the predictions of stellar evolution models as a more robust check of these stars' evolutionary status. We estimate the luminosity of each star from its absolute visual magnitude using bolometric corrections derived from a second-order polynomial fit to the calculated values of Houdashelt et al. (2000) over the range 5000 to 6000 K,

$$BC_{\rm V} = -5.30 + 0.00166\, T_{\rm e} - 1.31 \times 10^{-7}\, T_{\rm e}^2. \quad (1)$$

Fig. 7 plots the stars in the HR diagram with the theoretical models of Girardi et al. (2000).

Although the majority of estimated effective temperatures and luminosities are consistent with theoretical predictions for young, solar-metallicity, solar-mass stars there are eight stars (HD 1835, HD 10780, HD 11131, HD 43162, HD 73350, HD 97334, HD 130948, and HD 165185) whose measured luminosities and temperatures displace them from the solar-metallicity zero-age main seqence. A high-metallicity explanation is inconsistent with the spectroscopy-based abundance values presented here (-0.14 to +0.17 dex). In addition, these objects have anomalously low estimated surface gravities with $\log g \sim 4.1$ (Fig. 8). HD 118972 also has a low $\log g$ but lies on the main sequence: The large errors in the surface gravity indicate a poor fit to the stellar atmosphere model. HD 10780 has already been identified as an old star by virtue of its slow rotation compared to the rest of the sample (Gaidos et al. 2000). However, the remaining seven suspect stars are enigmatic: They display all the relevant characteristics of stellar youth, including high coronal X-ray luminosity, high chromospheric emission in the Ca II H and K lines, rapid rotation, and high lithium abundance (Gaidos et al. 2000). Two stars (HD 73350 and 97334) are putative members of the Hyades cluster and the Local Association, respectively (see §5.3).

The mass of a star can be uniquely derived from the effective temperature T, bolometric luminosity L, and surface gravity g using the relationship

$$M = \frac{gL}{4\pi G\sigma T^4}, \quad (2)$$

where G and σ are the gravitational and Stefan-Boltzmann constants. This can be re-expressed in terms of the parallax π and visual magnitude V (Fuhrmann et al. 1998):

$$\log \pi = 0.5([g]-[M])-2[T_{\rm e}]-0.2(V+BC_{\rm V}+0.26), \quad (3)$$

where $[X] = \log (X/X_{\odot})$. However, stellar evolution theory predicts that only some combination of M, L, T_e, and $\log g$ are possible. Theoretical evolution tracks can be used to check the consistency of these parameters (Allende-Prieto et al. 1999). Fig. 9 compares derived values of mass-luminosity pairs with Girardi et al. isochrones. With the exception of HD 1835, the derived mass and luminosity values of suspect stars are inconsistent with their main-sequence status. Stellar luminosity is estimated from accurate *Hipparcos* astrometric and photometry combined with a small bolometric correction. Instead, our T_e and/or $\log g$ estimates for these stars appear to be problematic.

Allende-Prieto & Lambert (1999) estimated atmosphere parameters for fifteen of our program stars using Eqn. 2 and stellar model predictions: Our measurements of $\log g$ and effective temperature and their estimates are discrepant by about 0.3 dex and 100 K, respectively. Error covariance between T_e and $\log g$ might then explain the trend seen in Fig. 1. One possibility is that the chromospheric activity has effected certain Fe lines and corrupted estimates of surface gravity. However, we found no significant correlation between stellar activity level and $\log g$ values. Paradoxically, the photometric estimates of effective temperature for these stars are in agreement with the spectroscopy-based results. We note that of three observations of HD 1237 on successive nights using the same telescope, instrument, observer, and data reduction procedure, the third produced an anomalously low $\log g$ estimate but a consistent temperature, metallicity, and microturbulence parameter (Gonzalez et al. 2001).

5.2. Microturbulence

The microturbulence parameter ξ_t for all of these stars is equal to or exceeds 1 km sec^{-1}. The sample mean is 1.30 km sec^{-1} with a standard deviation of 0.15 km sec^{-}. These values are distinctly higher than those obtained for older G-type stars by Gonzalez et al. (2001), using the identical analysis procedures (Fig. 10). The enhanced *macroturbulence* velocity dispersions of magnetically active stars were noted by Saar & Osten (1997). We compared our values with the predictions of the empirical relation derived by Feltzing & Gustafsson (1998) from measurements of 12 metal-rich G and K dwarf stars;

$$\xi_t = 4.5 \times 10^{-4} T_{\rm e} - 0.31 \log g. \quad (4)$$

The actual values exceed the predicted values by an average of only 0.14 km sec^{-1} and there is significant scatter (reduced χ^2 of 4.3). While this latter comparison suggests that the measured microturbulence parameters for these stars are not too abnormal, we caution that differences in the derivation procedure may limit the validity of this conclusion.

5.3. Abundances and Kinematics

Some of these young stars have been previously related to open clusters or co-moving groups via common space motions (Gaidos et al. 2000). One of the objectives of our abundance measurements was to determine if there is a link between association by space motion and association by elemental abundances. Two stars (HD 73350 and HD 180161) were identified as potential members of the Hyades cluster based on space motions (Gaidos et al. 2000). The [Fe/H] values reported here are also consistent with such membership (Fig. 11). Furthermore, the solar values of [Si/Fe] for these two stars agree with measurements on late F-type stars in the Hyades (Varenne & Monier 1999). This concordance allows us to assign a Hyades age ($\sim$ 650 Myr ; Perryman et al. 1998) to HD 73350 and HD 180161 with greater confidence. The latter star, at a distance of 20 pc, would be the closest known solar-mass member of the Hyades cluster.

The seven candidate members of the Ursa Major kinematic group (Gaidos et al. 2000) exhibit a wider range of [Fe/H] values that are still consistent with previous estimates of the metallicity distribution (Soderblom & Mayor 1993) (Fig. 12). A possible exception is HD 41593, which has an [Fe/H] of 0.06 ± 0.04. The dispersion of the stars about the Soderblom & Mayor average [Fe/H] of -0.08 is 0.10 dex, consistent with the previously estimated dispersion and significantly larger than the measurement errors ($\chi^2 = 27.5$, N = 5). Thus

there is *significant* variation in the [Fe/H] values within the Ursa Majoris kinematic group. If these stars are indeed coeval and originate from the same molecular cloud, then that cloud of origin must either have been heterogeneous with respect to Fe abundance (e.g., as a result of injection of material from previous generations of forming stars) or that Fe segregated out with varying degrees of efficiency in the cloud.

In principle, these two mechanisms can be distinguished by examining the distribution of [Si/Fe] values. Silicon and iron are contributed by different mass ranges of stars and it seems implausible that inhomogeneities produced by stellar mass loss would occur such that variations in [Fe/H] would not be accompanied by variations in [Si/Fe]. On the other hand, local variation in abundance that does not discriminate between Si and Fe (i.e., grain removal by radiation pressure) would produce constant [Si/Fe] in the resulting stellar population. The average [Si/Fe] for these seven stars is +0.02 and there is no significant dispersion about this mean. This observation supports the second mechanism.

Six stars have space motions consistent with membership in a second kinematic group known as the "Local Association" (Gaidos et al. 2000). (Note that HD 10008 was previously omitted because of a computational error). The existence of the Local Association was first suggested by Eggen (1983) and later re-identified in surveys of active and lithium-rich stars (Jeffries & Jewell 1993; Jeffries 1995). Although a link has been suggested with the Pleiades cluster, the relative motion between the Pleiades cluster and the Local Association is significant; 8.8 km sec^{-1} (Gaidos et al. 2000). The age-related properties of Local Association stars are also inconsistent with a Pleiades age of ~ 100 Myr (Gaidos et al. 2000). However, the Gaidos sample includes two young solar analogs (HD 82443 and HD 113449) with space motions similar to that of the Pleiades. HD 82443 (DX Leo) has already been suggested as a nearby Pleiades member (Soderblom & Clements 1987) and its chromospheric activity and X-ray luminosity is suggestive of a very young age. Unfortunately, line filling by chromospheric emission prevented accurate determination of the photosphere parameters or elemental abundances of this star.

The Fe abundances derived for the six previously-identified Local Association members span the range -0.02 to +0.11 while HD 113449 has [Fe/H] $= -0.06 \pm 0.05$. Values of [Na/Fe], [Mg/Fe], [Si/Fe], [Ca/Fe], [Ti/Fe], and [Ni,Fe] averaged over the Local Association members are -0.10, -0.11, -0.02, +0.01, -0.02, and -0.14, respectively. In particular, the Local Association stars appear to occupy a distinct part of a [Si/Fe] vs. [Fe/H] plot (Fig. 13), although not all of the stars in that region are members. With the possible exception of Ni, the abundance pattern of HD 113449 is statistically indistinguishable from that of the Local Association average. In particular, both have low Na and Mg abundances relative to Fe. The difference between the mean space motion of the Local Association and HD 113449 is 11 km sec^{-1}: However most of this is the difference in velocities along the relatively unconstrained axis perpendicular to the galactic plane. The chemical and kinematic similarity suggests a genetic relationship between HD 113449 and the members of the Local Association.

Boesgaard & Friel (1990) obtained an average [Fe/H] of -0.02 for 12 Pleiades F stars, Cayrel et al. (1985) found [Fe/H] = +0.13 for 4 G dwarfs, and King et al. (2000) estimated an average of [Fe/H] = 0.06 for two cool (late K) dwarfs. This broad range of metallicities is consistent with the Local Association members although HD 113449 is relatively metal poor. Detailed abundance data for Pleiades stars is scarce; the average of the two cool dwarfs analyzed by King et al. show an abundance pattern that is strikingly different, with solar [Mg] but depletion of Ca and Ti. However, it is not known if these stars are typical and a proper comparison with the Pleiades cluster will require abundance data for many more *bona fide* members.

We are grateful to the personnel of KPNO, especially D. Willmarth, for courteous and professional assistance in the spectroscopic observations. We also acknowledge the constructive comments of two anonymous reviewers. EJG was supported by the NASA Astrobiology Program and GG was supported, in part, by a grant from the Kenilworth Fund of the New York Community Trust. This publication makes use of data products from the Two Micron All Sky Survey, which is a joint project of the University of Massachusetts

and the Infrared Processing and Analysis Center/California Institute of Technology, funded by the National Aeronautics and Space Administration and the National Science Foundation. The SIMBAD database, maintained by the Centre de Données astronomiques de Strasbourg (CDS), and NASA's Astrophysics Data Systems Bibliographic Services were used extensively.

REFERENCES

Abt, H. A., & Willmarth, D. 1994, ApJS, 94, 677

Allende-Prieto, C., & Lambert, D. L. 1999, A&A, 353, 555

Allende-Prieto, C., Garcia-Lopez, R. J., Lambert D. L., & Gustafsson B. 1999, ApJ, 527, 879

Amando, P. J., Doyle, J. G., & Byrne, P. B. 2000, MNRAS, 314, 489

Bell, R. A., & Gustafsson, B. 1989, MNRAS, 236, 653

Blackwell, D. E., & Lynas-Gray, A. E. 1998, A&AS, 129, 505

Boesgaard, A. M., & Friel, H. D. 1990, ApJ, 351, 467

Cayrel, R., Cayrel de Strobel, G., & Campbell, B. 1985, A&A, 146, 249

Cayrel de Strobel, G., Soubiran, C., Friel, E. D., Ralite, N., & Francois, P. 1997, A&AS, 124, 299

Chen, Y. Q., Nissen, P. E., Zhao, G., Zhang, H. W., & Benoni, T. 2000, A&A, 141, 491

Cumming, A., Marcy, G. W., Butler, R. P. 1999, ApJ, 526, 890

Decin, G., Dominik, C., Marfait, K., Mayor, M., & Waelkens, C. 2000, A&A, 357, 533

Drake, J. J., & Smith, G. 1993, ApJ, 412, 797

Edvardsson, B., Andersen, J., Gustafsson, B., Lambert, D. L, Nissen, P. E., & Tomkin, J. 1993, A&A, 275, 101

Eggen, O. J. 1983, AJ, 88, 642

Favata, F., Micela, G. & Sciortino, S. 1997, A&A, 322, 131

Feltzing, S. & Gonzalez, G. 2001, A&A, 367, 253

Feltzing, S., & Gustafsson, B. 1998, A&A, 129, 237S

Fuhrmann, K., Pfeiffer, M. J., & Bernkopf, J. 1998, A&A, 336, 942

Gaidos, E. J. 1999, ApJ, 510, L131

Gaidos, E. J. 1998, PASP, 110, 1259

Gaidos, E. J., Henry, G. W., & Henry, S. M., 2000 AJ, 120, 1006

Gezari, D. Y., Pitts, P. S., & Schmitz, M. 1993, NASA RP-124, (Washington, DC: NASA)

Girardi, L., Bressan, A., Bertelli, G., & Chiosi, C. 2000, A&A, 141, 371

Glushneva, I. N., Shenavrin, V. I., Roschina, L. A. 2000, A. Rep. 44, 246

Gonzalez, G., Laws, C., Tyagi, S., & Reddy, B. E. 2001, AJ, 121, 432

Gonzalez, G., & Vanture, A. D. 1998, A&A, 339, L29

Gustafsson, B., Karlsson, T., Olsson, E., Edvardsson, B., & Ryde, N. 1999, A&A, 342, 426

Habing, H. J., et al. 2001, A&A, 365, 545

Hobbs, L. M. 1985, ApJ, 290, 284

Houdashelt, M. L., Bell, R. A., & Sweiger, A. V. 2000, AJ, 119, 1448

Jeffries, R. D., & Jewell, S. J. 1993, 264, 106

Jeffries, R. D. 1995, MNRAS, 273, 559

King, J. R. 2000, AJ, 120, 1056

King, J. R., Soderblom, D. R., Fischer, D., & Jones, B. F. 2000, ApJ, 533, 944

Kurucz, R. L. 1992, in IAU Symposium 149, The Stellar Populations of Galaxies, ed. B. Barbuy & A. Renzini (Dordrecht: Kluwer)

Kurucz, R. L. 1993, CD-ROM 13, ATLAS 9 Stellar Atmosphere Programs and 2 km/s Grid (Cambridge: Smithsonian Astrophys. Obs.)

Moshir, M., et al. 1992, Explanatory Supplement to the *IRAS* Faint Source Survey, Version 2, JPL D-100015 JPL, Pasadena.

Naef, D., Mayor, M., Pepe, F., Queloz, D., Udry, S., & Burnet, M. 2001, A&A, 375, 205

Ohnaka, K., Tsuji, T., & Aoki, W. 2000, A&A, 353, 528

Ottmann, R., Pfeiffer, M. J., & Gehren, T. 1998, A&A, 338, 661

Perryman, M. A. C., Brown, A. G. A., Lebreton, Y., Gomez, A., Turon, C., Cayrel de Strobel, G., Mermilliod, J. C., Robichon, N., Kovalevsky, J., & Crifo, F. 1998, A&A, 331, 81

Perryman, M. A. C. 1997, ESA SP-402: Hipparcos - Venice '97, 402, 1

Press, W. H., Flannery, B. P., Teukolsky, S. A. & W. T. Vetterling, *Numerical Recipes: The Art of Scientific Computing*, Cambridge: Cambridge University Press (1986)

Saar, S. H., & Osten, R. A. 1997, MNRAS, 284, 803

Santos, N. C., Israelian, G., & Mayor, M. 2001, A&A, 373, 1019S

Sneden, C. 1973, Ph. D. Thesis, Univ. Texas Austin

Soderblom, D. R., King, J. R., Hanson, R. B., Jones, B. F., Fischer, D., Stauffer, J. R., & Pinsonneault, M. H. 1998, ApJ, 504, 192

Soderblom, D. R., & Mayor, M. 1993, AJ, 105, 226.

Soderblom, D. R., & Clements, S. D. 1987, AJ, 95, 580.

Steenbock, W. & Holweger, H. 1981, A&A, 99, 192S

Strassmeier, K. G., Washuettla, A., Granzer, T., Scheck, M., & Weber, M. 2000, A&A, 142, 275S

Timmes, F. X., Woosley, S. E., & Weaver, T. A. 1995, ApJS, 98, 617

Tokovinin, A. A. 1992, A&A, 256, 121

Tomkin, J., Woolf, V. M., Lambert, D. L., & Lemke, M. 1995, AJ, 109, 2204

Varenne, O., & Monier, R. 1999, A&A, 351, 247

Wyse, R. F. G., & Gilmore, G. 1985, AJ, 110, 2771

Zboril, M., & Byrne, P. B. 1998, MNRAS, 299, 753.

This 2-column preprint was prepared with the AAS LaTeX macros v5.0.

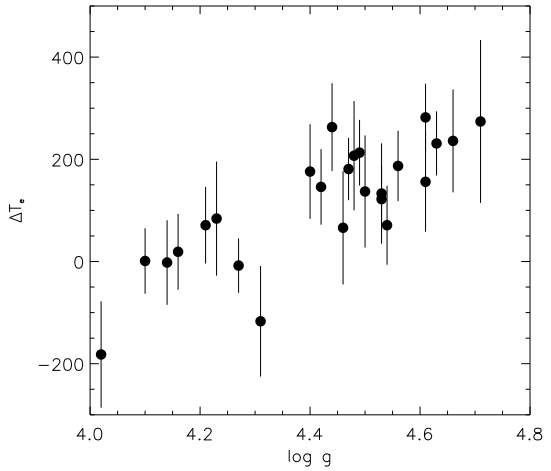

Fig. 1.— Difference between the spectroscopic and photometric effective temperature estimates vs. surface gravity for the program star sample.

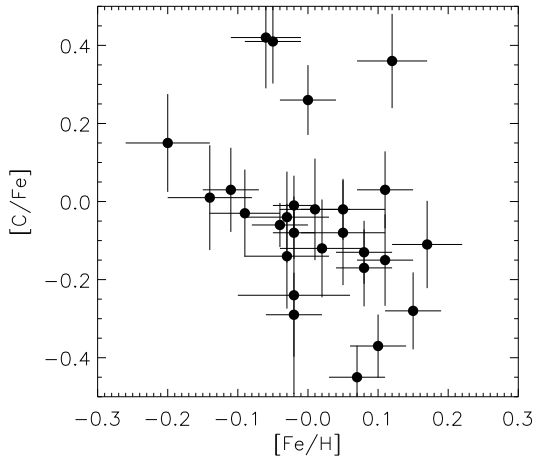

Fig. 3.— Abundance of C relative to Fe in the program star sample.

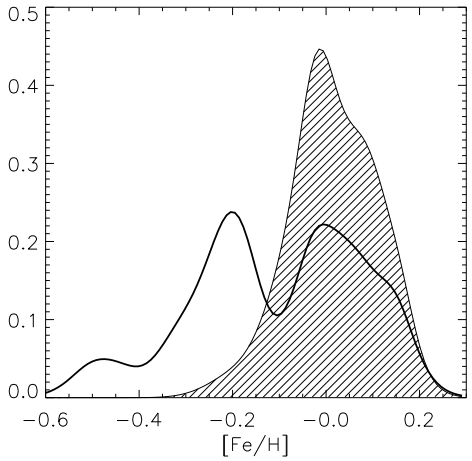

Fig. 2.— Distribution of [Fe/H] among the sample of 33 program stars (shaded curve). This is calculated by summing the (normal) error distribution for each measurement and is in units of the fraction of the sample per 0.1 dex. The heavy curve is the [Fe/H] distribution of the volume-limited sample of Santos et al. (2001)

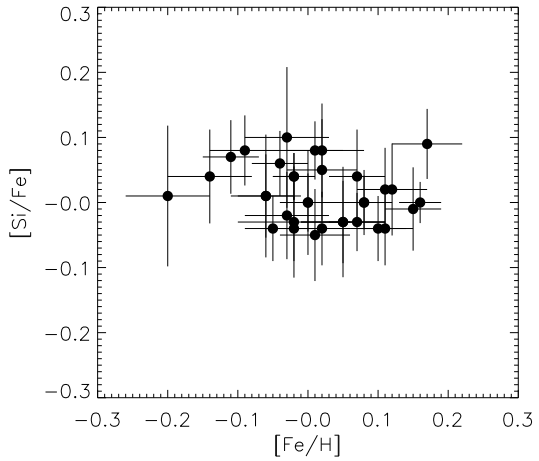

Fig. 4.— Abundance of Si relative to Fe.

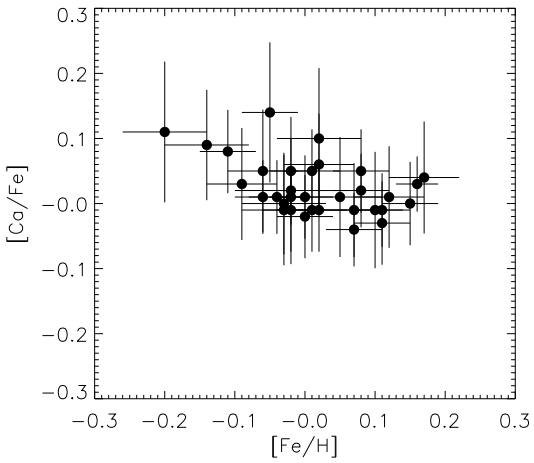

Fig. 5.— Abundance of Ca relative to Fe.

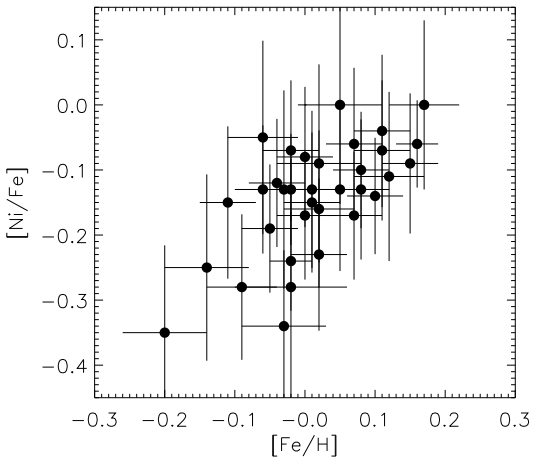

Fig. 6.— Abundance of Ni relative to Fe.

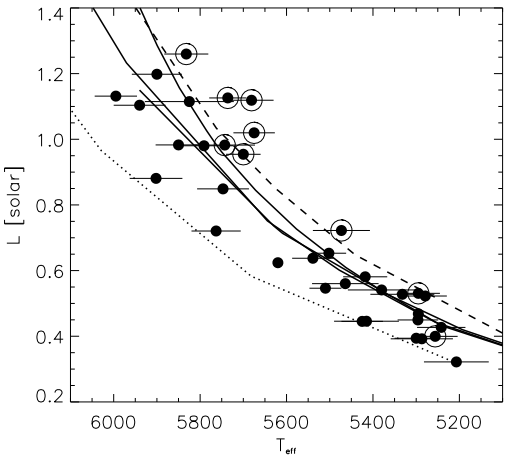

Fig. 7.— Hertzsprung-Russell diagram (luminosity vs. effective temperature) for the program stars. The three solid lines (from lower to upper) are 0.8-1.2 $M_\odot$ solar-metallicity isochrones for ages of 100, 800, and 4500 million years from Girardi et al. (2000). Also plotted are the 800-million year isochrones for $Z = 0.008$ (dotted) and $Z = 0.03$ (dashed). The circled points are the stars with anomalously low surface gravity discussed in the text.

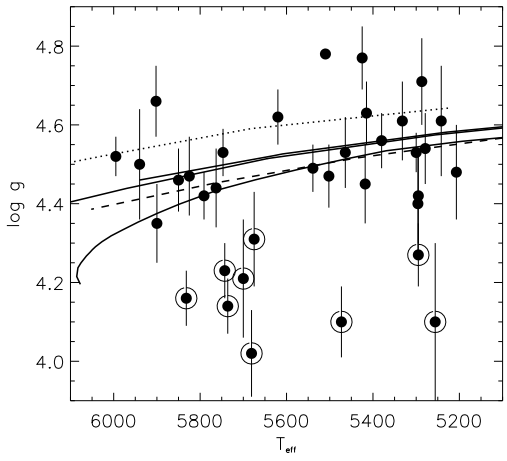

Fig. 8.— Surface gravity vs. effective temperature for the program stars. Girardi et al. (2000) isochrones are as in Fig. 7.

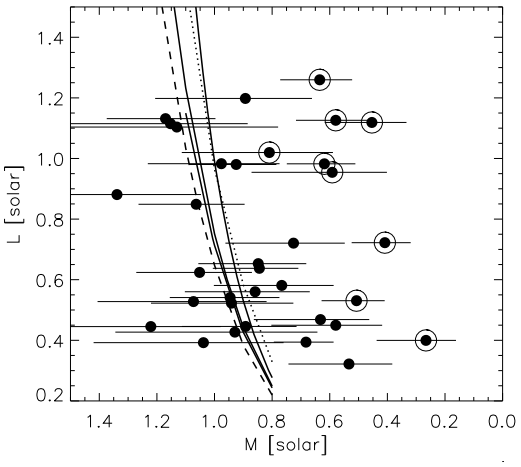

Fig. 9.— Stellar luminosity (derived from absolute magnitude and a bolometric correction) vs. stellar mass (derived from effective temperature, surface gravity, and luminosity) of the program stars expressed in solar units. Girardi et al. isochrones are plotted as in Fig. 7. The circled stars are nearly all inconsistent with the model.

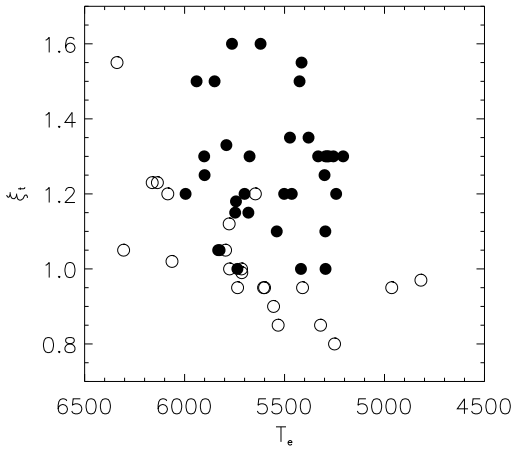

Fig. 10.— Derived microturbulence parameter ξ_t (in km sec^{-1}) vs. effective temperature for the young solar analog stars (filled points) compared to a sample of older solar-type stars with planets analyzed in Gonzalez et al. (2001) (empty points). The ξ_t values for the young stars are systematically higher for the same effective temperature.

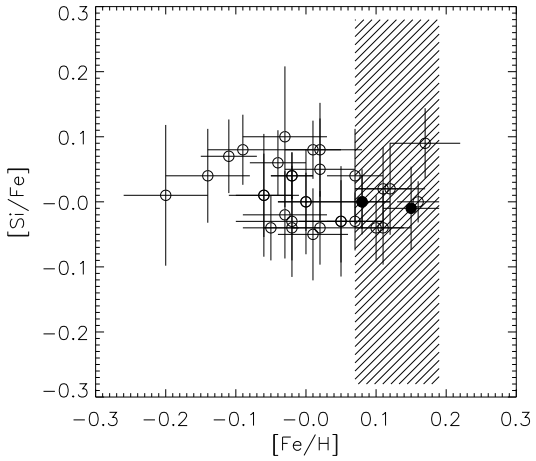

Fig. 11.— Same as Fig. 4, except that two Hyades cluster candidate members are plotted as filled circles. The hatched region is the range of [Fe/H] observed in the Hyades cluster within one standard deviation of the mean.

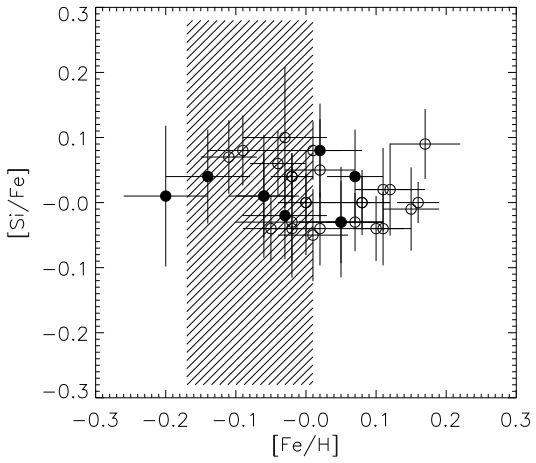

Fig. 12.— Same as Fig. 4, except that seven Ursa Major kinematic group members are plotted as filled circles. The hatched region is the range of the group metallicity within one standard deviation of the mean (Soderblom & Mayor 1993).

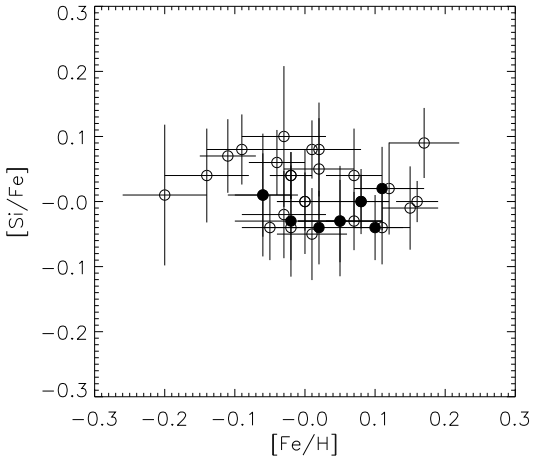

Fig. 13.— Same as Fig. 4, except that six Local Association kinematic group members and HD 113449 are plotted as filled circles (HD 113449 is the far left point).

TABLE 1
ATOMIC DATA FOR LINES

SPECIES ($\epsilon_\odot$)	λ_0 ($\AA$)	χ_1 (eV)	log gf
C I (8.56).....	6587.620	8.53	-1.08
Na I (6.33)....	6154.230	2.10	-1.58
	6160.750	2.10	-1.26
Mg I (7.58)....	5711.100	4.34	-1.71
Si I (7.55)....	6125.030	5.61	-1.54
	6145.020	5.61	-1.42
	6721.840	5.86	-1.14
	6721.850	5.86	-1.14
S I (7.21).....	6052.680	7.87	-0.44
Ca I (6.36)....	5867.570	2.93	-1.62
	5867.572	2.93	-1.62
	6166.440	2.52	-1.13
Ti I (4.99)....	5965.835	1.88	-0.38
	5965.840	1.88	-0.38
	6126.220	1.07	-1.41
	6261.110	1.43	-0.46
	6261.220	1.43	-0.46
Fe I (0.00)....	5852.220	4.55	-1.18
	5853.160	1.48	-5.18
	5855.090	4.61	-1.52
	5856.100	4.29	-1.56
	5956.700	0.86	-4.55
	6027.060	4.07	-1.09
	6034.090	4.31	-2.26
	6056.010	4.73	-0.40
	6079.070	4.65	-1.02
	6089.570	5.02	-0.86
	6093.700	4.61	-1.34
	6096.670	3.98	-1.81
	6098.310	4.56	-1.74
	6120.250	0.91	-5.88
	6151.620	2.18	-3.29
	6157.790	4.07	-1.25
	6159.440	4.61	-1.87
	6165.360	4.14	-1.47
	6180.260	2.73	-2.61
	6188.050	3.94	-1.61
	6200.320	2.61	-2.44
	6226.740	3.88	-2.03
	6229.230	2.84	-2.82
	6240.710	2.22	-3.32
	6265.140	2.18	-2.57
	6380.740	4.19	-1.32
	6392.610	2.28	-4.01
	6499.010	0.96	-4.62
	6581.220	1.48	-4.66
	6591.380	4.59	-1.98
	6608.100	2.28	-4.01
	6627.620	4.55	-1.44
	6653.920	4.15	-2.41
	6703.580	2.76	-3.01
	6710.300	1.48	-4.80
	6725.430	4.10	-2.18
	6726.740	4.61	-1.04
	6733.150	4.64	-1.45
	6739.520	1.56	-4.90
	6750.160	2.42	-2.62
	6752.710	4.64	-1.20
	6786.930	4.19	-1.95
	6820.370	4.64	-1.17
	6839.840	2.56	-3.36
	6855.720	4.61	-1.73
	6861.950	2.42	-3.80
	6862.500	4.56	-1.35
	5806.730	4.61	-0.90

TABLE 1—*Continued*

SPECIES ($\epsilon_\odot$)	λ_0 ($\AA$)	χ_1 (eV)	log gf
Fe II.....	5425.260	3.20	-3.18
	5991.380	3.15	-3.48
	6084.170	3.20	-3.75
	6149.250	3.89	-2.70
	6247.560	3.89	-2.30
	6369.450	2.89	-4.11
Ni I (6.25)....	6767.780	1.83	-2.09

TABLE 2
PHOTOSPHERE PARAMETERS FROM SPECTROSCOPY

HD	S.T.[a]	T_e	log g	ξ_t (km sec^{-1})	[Fe/H]	n_{FeI}	n_{FeII}
166	K0	5620(40)	4.62(0.07)	1.60(0.11)	0.10(0.04)	44	7
1237[b]	G6	5502(48)	4.47(0.08)	1.20(0.09)	0.14(0.04)	...	...
1835	G3	5675(60)	4.31(0.12)	1.30(0.13)	0.17(0.05)	44	5
7590	G0	5940(75)	4.50(0.14)	1.50(0.23)	-0.03(0.06)	39	6
10008	G5	5415(50)	4.63(0.08)	1.55(0.14)	0.02(0.04)	45	5
10780	K0	5295(40)	4.27(0.08)	1.00(0.07)	-0.02(0.03)	46	5
11131	G0	5700(60)	4.21(0.15)	1.20(0.13)	-0.09(0.05)	42	5
20630	G5	5747(49)	4.53(0.06)	1.15(0.09)	0.11(0.04)	46	6
26923	G0	5995(68)	4.52(0.05)	1.20(0.17)	0.05(0.06)	42	5
30495	G3	5791(37)	4.42(0.06)	1.33(0.09)	-0.02(0.03)	42	5
36435[c]	G8	5510	4.78	1.15	0.03	...	...
37394	K1	5295(47)	4.42(0.12)	1.30(0.09)	0.08(0.04)	44	6
41593	K0	5296(66)	4.40(0.12)	1.10(0.12)	0.07(0.04)	47	4
43162	G5	5473(56)	4.10(0.09)	1.35(0.14)	-0.11(0.04)	40	6
52698	K1	5242(61)	4.61(0.14)	1.20(0.11)	0.12(0.05)	46	6
59967	G4	5902(57)	4.66(0.09)	1.30(0.14)	0.01(0.05)	45	5
63433	G5	5763(74)	4.44(0.10)	1.60(0.17)	0.02(0.06)	39	4
72760	G5	5332(53)	4.61(0.10)	1.30(0.10)	0.01(0.04)	45	5
72905	G1.5	5850(70)	4.46(0.08)	1.50(0.16)	-0.03(0.06)	47	6
73350	G0	5743(43)	4.23(0.07)	1.18(0.08)	0.08(0.04)	44	5
82443	K0	...	...	...	...	...	...
97334	G0	5736(75)	4.14(0.07)	1.00(0.15)	0.05(0.06)	45	6
109011	K2	5207(72)	4.48(0.12)	1.30(0.14)	-0.20(0.06)	38	6
113449	G6	5287(78)	4.71(0.11)	1.30(0.15)	-0.06(0.05)	44	5
116956	G9	5380(52)	4.56(0.07)	1.35(0.11)	0.11(0.04)	45	5
118972	K2	5256(48)	4.10(0.20)	1.30(0.09)	-0.05(0.04)	42	5
128400	G5	...	...	...	...	...	...
128987	G6	5539(51)	4.49(0.06)	1.10(0.12)	0.00(0.04)	46	5
130948	G1	5832(50)	4.16(0.07)	1.05(0.11)	-0.04(0.04)	42	5
135599	K0	5300(48)	4.53(0.05)	1.25(0.10)	-0.06(0.04)	44	5
141272	G8	5425(51)	4.77(0.08)	1.50(0.11)	0.00(0.04)	43	6
152391	G8	5418(51)	4.45(0.10)	1.00(0.09)	-0.02(0.04)	45	5
165185	G5	5681(77)	4.02(0.11)	1.15(0.17)	-0.14(0.06)	38	6
180161	G8	5464(58)	4.53(0.09)	1.20(0.09)	0.15(0.04)	44	5
203244	G5	...	...	...	...	...	...
206860	G0	5900(103)	4.35(0.10)	1.25(0.28)	-0.02(0.08)	40	5
217813	G5	5825(50)	4.47(0.10)	1.05(0.11)	0.07(0.04)	41	6
220182	K1	5279(69)	4.54(0.09)	1.30(0.12)	0.02(0.05)	37	4

[a]From SIMBAD

[b]From Gonzalez et al. (2001)

[c]From Santos et al. (2001)

TABLE 3
PHOTOSPHERE PARAMETERS FROM PHOTOMETRY

HD	T_e	$R/R_\odot$	N	χ^2
166	...	...	...	...
1237	...	...	...	...
1835	5792(90)	0.951(0.020)	15	26.9
7590	5803(80)	0.990(0.011)	2	...
10008	5184(38)	0.810(0.009)	4	8.9
10780	5303(35)	0.818(0.007)	4	5.3
11131	5629(45)	0.986(0.011)	4	13.5
20630	5614(85)	0.940(0.021)	14	13.3
26923	...	...	...	...
30495	...	...	...	...
36435	5277(28)	0.871(0.007)	2	...
37394	5149(57)	0.834(0.019)	5	1.9
41593	5120(65)	0.830(0.013)	2	...
43162	5472(31)	0.901(0.008)	2	...
52698	4960(25)	0.877(0.008)	2	...
59967	5666(83)	0.944(0.019)	14	17.5
63433	5500(44)	0.910(0.010)	4	8.7
72760	5176(82)	0.870(0.012)	4	5.5
72905	5784(86)	0.946(0.014)	5	2.1
73350	5659(103)	0.991(0.027)	2	...
82443	5142(32)	0.839(0.008)	3	0.13
97334	5738(35)	1.025(0.010)	2	...
109011	5000(79)	0.850(0.011)	3	32.5[a]
113449	5013(139)	0.865(0.027)	3	6.6
116956	5193(45)	0.885(0.015)	4	4.0
118972	...	...	...	...
128400	...	...	...	...
128987	5326(39)	0.916(0.009)	4	11.7
130948	5813(55)	1.058(0.014)	5	6.9
135599	...	...	...	...
141272	...	...	...	...
152391	...	...	...	...
165185	5863(70)	0.968(0.013)	10	10.0
180161	5342(30)	0.844(0.008)	2	...
203244	...	...	...	...
206860	...	...	...	...
217813	5644(35)	1.068(0.010)	2	...
220182	5208(35)	0.854(0.008)	4	46.1

[a]Possible spectroscopic binary

TABLE 4
DERIVED ELEMENTAL ABUNDANCES

HD	[Fe/H]	[C/H]	[Na/H]	[Mg/H]	[Si/H]	[S/H]	[Ca/H]	[Ti/H]	[Ni/H]
166	0.10(0.04)	-0.27(0.07)	0.09(0.04)	-0.03(0.07)	0.06(0.03)	-0.01(0.07)	0.09(0.08)	0.13(0.05)	-0.04(0.08)
1237	0.16(0.03)	···	0.08(0.03)	0.09(0.05)	0.16(0.01)	0.24(0.05)	0.19(0.03)	0.11(0.03)	0.10(0.06)
1835	0.17(0.05)	0.06(0.10)	0.01(0.07)	0.10(0.10)	0.26(0.02)	0.37(0.09)	0.21(0.07)	0.12(0.07)	0.17(0.12)
7590	-0.03(0.06)	-0.17(0.12)	-0.22(0.07)	-0.14(0.12)	0.07(0.09)	-0.09(0.11)	-0.04(0.06)	-0.16(0.08)	-0.16(0.14)
10008	0.02(0.04)	···	-0.16(0.04)	-0.09(0.10)	-0.02(0.04)	0.30(0.10)	0.01(0.05)	0.02(0.07)	-0.21(0.11)
10780	-0.02(0.03)	-0.03(0.07)	-0.09(0.03)	-0.02(0.07)	0.02(0.02)	···	0.03(0.04)	-0.02(0.05)	-0.15(0.08)
11131	-0.09(0.05)	-0.12(0.10)	-0.23(0.04)	-0.17(0.10)	-0.01(0.02)	···	-0.06(0.07)	-0.15(0.06)	-0.37(0.10)
20630	0.11(0.04)	-0.04(0.11)	-0.04(0.03)	-0.04(0.08)	0.07(0.04)	···	0.10(0.04)	0.11(0.08)	0.04(0.10)
26923	0.05(0.06)	-0.03(0.12)	-0.11(0.10)	-0.03(0.10)	0.02(0.06)	-0.06(0.10)	-0.07(0.35)	0.02(0.12)	-0.08(0.11)
30495	-0.02(0.03)	-0.10(0.06)	-0.09(0.05)	-0.13(0.06)	0.02(0.02)	-0.07(0.06)	-0.01(0.03)	0.01(0.08)	-0.26(0.07)
37394	0.08(0.04)	-0.09(0.09)	0.03(0.08)	0.00(0.09)	0.08(0.03)	0.00(0.09)	0.13(0.05)	0.09(0.07)	-0.05(0.10)
41593	0.07(0.04)	···	-0.14(0.06)	0.02(0.10)	0.11(0.06)	0.10(0.10)	0.06(0.06)	0.14(0.09)	0.01(0.11)
43162	-0.11(0.04)	-0.08(0.10)	-0.05(0.09)	-0.03(0.10)	-0.04(0.04)	-0.04(0.09)	-0.03(0.05)	-0.10(0.08)	-0.26(0.11)
52698	0.12(0.05)	0.48(0.11)	0.04(0.13)	0.07(0.11)	0.14(0.05)	0.04(0.11)	0.13(0.06)	0.31(0.10)	0.01(0.12)
59967	0.01(0.05)	-0.01(0.12)	-0.14(0.08)	-0.12(0.09)	-0.04(0.05)	0.20(0.09)	0.00(0.04)	0.07(0.09)	-0.12(0.11)
63433	0.02(0.06)	-0.10(0.11)	-0.10(0.12)	-0.02(0.12)	0.10(0.04)	-0.15(0.11)	0.12(0.09)	0.08(0.08)	-0.07(0.14)
72760	0.01(0.04)	···	0.02(0.18)	-0.13(0.09)	0.09(0.02)	0.27(0.09)	0.06(0.05)	0.00(0.07)	-0.14(0.10)
72905	-0.03(0.06)	-0.07(0.10)	-0.09(0.04)	-0.13(0.11)	-0.05(0.03)	···	-0.03(0.05)	-0.15(0.06)	-0.37(0.10)
73350	0.08(0.04)	-0.05(0.07)	-0.05(0.08)	0.04(0.07)	0.08(0.01)	-0.08(0.07)	0.10(0.04)	0.01(0.05)	-0.02(0.08)
97334	0.05(0.06)	0.03(0.05)	-0.03(0.04)	0.01(0.12)	0.02(0.02)	0.08(0.11)	0.06(0.07)	-0.03(0.07)	0.05(0.14)
109011	-0.20(0.06)	-0.05(0.11)	-0.29(0.09)	-0.28(0.11)	-0.19(0.09)	···	-0.09(0.09)	-0.03(0.13)	-0.55(0.12)
113449	-0.06(0.05)	0.36(0.12)	-0.22(0.07)	-0.17(0.12)	-0.05(0.08)	···	-0.01(0.08)	-0.02(0.10)	-0.11(0.14)
116956	0.11(0.04)	0.14(0.09)	-0.04(0.12)	-0.07(0.09)	0.13(0.05)	···	0.08(0.05)	0.08(0.07)	0.07(0.11)
118972	-0.05(0.04)	0.36(0.10)	-0.13(0.12)	0.12(0.10)	-0.09(0.03)	···	0.09(0.10)	0.02(0.07)	-0.24(0.09)
128987	0.00(0.04)	0.26(0.08)	-0.12(0.04)	-0.08(0.08)	0.00(0.02)	···	0.01(0.05)	-0.01(0.06)	-0.08(0.10)
130948	-0.04(0.04)	-0.10(0.04)	-0.20(0.08)	-0.07(0.07)	0.02(0.03)	-0.03(0.07)	-0.03(0.04)	-0.19(0.05)	-0.16(0.09)
135599	-0.06(0.04)	0.50(0.71)	-0.23(0.08)	-1.27(0.00)	-0.05(0.05)	···	-0.05(0.04)	-0.01(0.06)	-0.19(0.09)
141272	0.00(0.04)	···	-0.22(0.05)	-0.18(0.08)	0.00(0.07)	···	-0.02(0.05)	0.03(0.07)	-0.17(0.09)
152391	-0.02(0.04)	-0.31(0.10)	-0.17(0.06)	-0.09(0.09)	-0.06(0.03)	-0.14(0.09)	-0.03(0.05)	-0.01(0.06)	-0.09(0.10)
165185	-0.14(0.06)	-0.13(0.12)	-0.34(0.08)	-0.08(0.12)	-0.10(0.04)	-0.46(0.11)	-0.05(0.06)	-0.31(0.08)	-0.39(0.13)
180161	0.15(0.04)	-0.13(0.09)	0.00(0.06)	0.05(0.09)	0.14(0.05)	0.08(0.09)	0.15(0.05)	0.15(0.07)	0.06(0.10)
206860	-0.02(0.08)	-0.26(0.24)	-0.16(0.06)	-0.13(0.16)	-0.05(0.03)	-0.08(0.14)	0.00(0.08)	-0.07(0.12)	-0.30(0.18)
217813	0.07(0.04)	-0.38(0.07)	-0.06(0.03)	-0.08(0.08)	0.04(0.02)	-0.23(0.07)	0.03(0.04)	-0.03(0.06)	-0.10(0.09)
220182	0.02(0.05)	1.38(0.10)	-0.17(0.07)	-0.11(0.10)	0.07(0.06)	···	0.08(0.06)	-0.04(0.10)	-0.14(0.11)